A study of the mixing state of black carbon in urban zone

M. Mallet,[1] J. C. Roger,[2] S. Despiau,[1] J. P. Putaud,[3] and O. Dubovik[4]

Received 2 July 2003; revised 1 December 2003; accepted 10 December 2003; published 21 February 2004.

[1] The knowledge of the mixing state of black carbon particle with other aerosol species is critical for adequate simulations of the direct radiative effect of black carbon particles and its effect on climate. This paper reports the investigation of the mixing state of black carbon aerosol in the urban zone. The study uses a combination of in situ and ground-based remote sensing observations conducted during the ESCOMPTE experiment, which took place in industrialized region in France in summer of 2001. The criteria we used for identifying mixing state relies on the known enhancement of absorption for aerosol composed by internal versus external mixtures of black carbon with weakly absorbing aerosol components. First, using in situ aerosol data, we performed Mie computations and reconstructed the single scattering albedo of aerosol for the two different mixing assumptions: black carbon mixed externally or internally with other aerosol species. Then, we compared the obtained values $\omega_{o,int}$ and $\omega_{o,ext}$ with the retrievals of ω_o from independent AERONET Sun-photometric measurements. The aerosol single scattering albedo ($\omega_{o,aer.}$) derived from the AERONET photometer observations (with the mean value equal to 0.84 ± 0.04) was found to be close to $\omega_{o,ext}$ reconstructed from in situ observation under assumptions of external mixture. This similarity between AERONET values and external mixture simulations was observed during all the days studied. Our conclusion on external mixture of black carbon aerosol with other particles in urban zone during ESCOMPTE (close to the pollution source) is coherent with observations made during other independent studies reported in a number of recent publications. *INDEX TERMS:* 0305 Atmospheric Composition and Structure: Aerosols and particles (0345, 4801); 0345 Atmospheric Composition and Structure: Pollution—urban and regional (0305); 1610 Global Change: Atmosphere (0315, 0325); 3359 Meteorology and Atmospheric Dynamics: Radiative processes; *KEYWORDS:* aerosol, black carbon, mixing state

Citation: Mallet, M., J. C. Roger, S. Despiau, J. P. Putaud, and O. Dubovik (2004), A study of the mixing state of black carbon in urban zone, *J. Geophys. Res.*, *109*, D04202, doi:10.1029/2003JD003940.

1. Introduction

[2] Anthropogenic aerosol particles have increased significantly over the industrial period because human activities and their effect on global warming represents, at present time, the largest source of uncertainty on the estimation of future climate [*Houghton et al.*, 2001]. Aerosol particles interfere with solar radiation by scattering it back to space and (or) by absorbing it into the atmospheric layer. These modifications of the energy input into the aerosol layer correspond to the "direct radiative effect" [*Haywood and Shine*, 1995]. These optical processes and the associated direct radiative forcing are directly related to the microphysical aerosol properties, and more especially to the number size distribution and the chemical composition of the particles. The estimation of the direct radiative forcing exerted by aerosol on climate is complex to quantify because anthropogenic particles are generally a complex mixing of different chemical components, among them sulfate, ammonium, nitrate, dust, sea salt, organic and black carbon are considered as the most important [*Hegg et al.*, 1997; *Putaud et al.*, 2000; *Ramanathan et al.*, 2001]. Each component is characterized by its own microphysical, chemical, and related optical properties, which lead to variable direct radiative forcing.

[3] During the last decade, several investigations have been focused on sulfate, which is suspected to decrease the globally averaged solar radiation received by the Earth-Atmosphere system. This top of atmosphere (TOA) direct "cooling" effect has been estimated by *Charlson et al.* [1992] at -0.40 Wm^{-2} but, according to *Houghton et al.* [2001], with an uncertainty factor of two. The most recent global models including other anthropogenic aerosols indicate a similar "cooling" effect of nitrates, (-0.02 Wm^{-2} by *Adams et al.* [2001]) and organic carbon (-0.02 to -0.09 Wm^{-2} by *Cooke et al.* [1999]). These aerosols mainly reflect the solar radiation back to space.

[4] On the contrary of these aerosol scattering species, black carbon particles behave differently and can, in addition with their scattering properties, absorb the solar radi-

[1]LEPI, Université de Toulon et du Var, La Valette du Var, France.
[2]LOCL/MREN, Université du Littoral Côte d'Opale, Dunkerque, France.
[3]Joint Research Centre, Ispra, Italy.
[4]NASA Goddard Space Flight Center, Greenbelt, Maryland, USA.

0148-0227/04/2003JD003940$09.00

ations what can change the sign of the TOA direct radiative forcing from negative to positive, depending of the surface albedo. Direct radiative forcing estimation of black carbon aerosols at TOA has been calculated in various recent studies and the estimated values range from about +0.16 to +0.20 Wm^{-2} [*Cooke et al.*, 1999; *Haywood et al.*, 1997; *Haywood and Ramaswamy*, 1998], which represents a considerable amount of heating of the atmosphere and a potential factor causing global warming.

[5] The uncertainty on the estimation of the black carbon direct radiative forcing comes predominantly from an unknown optical thickness (total amount of black carbon, size distribution, imaginary part of the refractive index) but also from its mixing state with other aerosols. The mixing state of a population of particles is often characterized by two extreme microphysical properties. One is called the external mixture, where, in the aerosol population, each particle consists of only one chemical substance. The other is an internal mixture, in which all particles contain a mixture of components from each of the sources [*Seinfeld and Pandis*, 1998]. *Ackerman and Toon* [1981] and more recently *Jacobson* [2001] indicated that when black carbon is associated with the scattering aerosol (as sulfate, nitrate, or organic carbon) in internal mixture, it could absorb more sunlight. Hence black carbon could exert a globally averaged "positive" direct radiative forcing of +0.27 Wm^{-2} in external mixture and +0.54 Wm^{-2} in internal mixture (in a coated core case). In the last case, *Jacobson* [2001] indicated that "the magnitude of the black carbon direct radiative forcing could exceed that due to CH_4, becoming the second most important component of global warming after CO_2".

[6] The known importance of accounting for the aerosol mixing state in evaluating aerosol forcing climatic impact stimulated numerous studies investigations aimed to quantify aerosol mixing. For example, *Hasegawa and Ohta* [2002] analysed individual particles on a carbon-covered nitrocellulose film by a transmission electron microscope. Hygroscopic measurements with the Tandem Differential Mobility Analyser (TDMA) technique also provide information on the mixing state of the aerosol, often showing the occurrence of two or more subpopulations with different hygroscopicity [*Wang et al.*, 2002; *Van Dingenen et al.*, 2002a, 2002b]. *Middlebrook et al.* [1998] used mass spectrometer measurements of individual aerosol particles to study the mixing state of aerosol. Nevertheless, the determination and accounting for black carbon mixing state with other aerosol species is very complex and not completely resolved yet.

[7] The aim of this study is to investigate the mixing state of black carbon with other aerosol species in urban environment. This work uses the dependence of the single scattering albedo, ω_o, to the mixing state of black carbon aerosol. Indeed, ω_o, which represents the ratio of light scattering to scattering + absorption, is shown in numerous studies to be very sensitive to this microphysical parameter [*Haywood and Shine*, 1995; *Lesins et al.*, 2002]. The principle of this work is to compute ω_o from in situ measurements for the two mixing state, internal and external (noted $\omega_{o,int}$ and $\omega_{o,ext}$) and to compare them with ω_o deduced from an independent optical measurement. Our computations of ω_o from the in situ measurements are based on the *Mie* [1908] theory, which allows deriving ω_o from the aerosol number size distribution and the refractive index (linked to the aerosol chemical composition) (see section 4). The optical estimation of ω_o used in this work was performed from the Sun-photometer measurements (see section 3.2). The results presented here are focused on an urban aerosol measured during the ESCOMPTE experiment [*Cros et al.*, 2004] described hereafter.

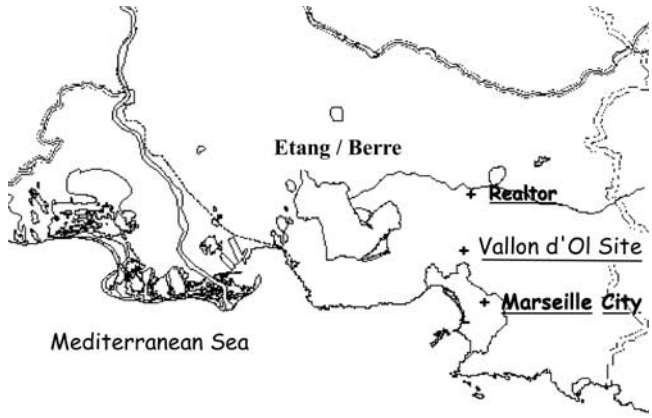

Figure 1. The Vallon d'Ol Site in peri urban zone of Marseille.

2. Experimental Campaign

[8] Between 4 June and 13 July 2001, the cooperative experiment ESCOMPTE was a field campaign devoted to constrain models of atmospheric pollution and transport of emissions [*Cros et al.*, 2004]. The main objective of the ESCOMPTE program is to establish a detailed database of primary pollutant emissions together with dynamics and chemistry of the atmosphere during high pollution events. The field campaign took place, over an area of 100 × 100 km, in a southeastern part of France involving the urban area of Marseille and the industrial complex of Fos-Berre (Figure 1). Due to urban and industrial emissions and due to a strong solar radiation, high and frequent pollution events are observed in this area. The data set acquired during this experiment will then be used to qualify and improve mesoscale models. During this period, several instruments were deployed in addition to the air quality network measurements performed by local agencies. Ground-based stations were operated in the domain and a ferry between France and Corsica was equipped with an air pollution station. Two aircrafts instrumented for dynamics and chemistry, constant volume balloons, radiosonde soundings, and wind profilers were operated simultaneously. The description of the ESCOMPTE campaign is presented in detail by *Cros et al.* [2004].

[9] Among the numerous objectives of this experiment, one concerned the physico-chemical characterisation of aerosol particles in urban and peri-urban zones. Measurements were mainly carried out during four IOPs (Intense Observation Period), which correspond to meteorological conditions favorable to pollution events, which can be summarized as follows: (1) anticyclonic conditions, (2) coastal breeze, (3) strong solar radiation leading to air temperature comprised between 25 and 30°C.

[10] Four pollution episodes (IOP 1, 2, 3, and 4 during 14–15 June, 22–26 June, 2–4 July and 10–12 July, respectively) corresponded with these meteorological conditions during the ESCOMPTE campaign. Results presented here are based upon a data set measured during these four IOPs in the peri-urban zone, called the "Vallon Dol" site, located 2 km north of Marseille and mainly polluted by the city traffic.

3. Aerosol Characteristics

3.1. Aerosol Size Distribution

[11] Anthropogenic aerosols are composed of a complex mixture of mineral dust, black carbon, and water-soluble particles such as ammonium sulfate, nitrates, sea salt, and organic matter. Size-segregated aerosol was collected at ambient relative humidity using a low-pressure eight-stage Berner impactor (LPI 80/0.05) loaded with prefired aluminium foils. The 50% aerodynamic cut-off diameters were 0.06, 0.125, 0.25, 0.5, 1, 2, 4, and 8 μm. The sampling duration was about 8 hours (1000 am to 1800 pm) during ESCOMPTE.

[12] The mass of carbon collected on the aluminium foils was determined using a thermal method (Evolved Gas Analysis, EGA), where samples are exposed successively to five increasing temperature plateaus up to 650°C in an oxygen-free carrier gas and then in an oxygen-rich carrier gas at 650–750°C [*Putaud et al.*, 2000]. The carbon evolved at T < 650°C in He is defined as OC but contains also carbonate, and the fraction evolved at T > 650°C in the oxidizing carrier gas is expected to be black carbon. However, due to possible charring during the analysis, the black carbon values obtained with this routine method can be highly overestimated. Therefore each sample was divided into two half foils, one of which was exposed at 340°C for 2 hours in an oxidizing carrier gas ($He:O_2$ 80:20). This thermal treatment was shown to remove most of the OC susceptible to be charred [*Cachier et al.*, 1989]. The carbon fraction evolved from the treated aliquot at T > 650°C was defined as BC. The detector was calibrated twice a day by injecting known amounts of pure CO_2 and the instrument overall response checked daily using a sodium oxalate standard. The analytical precision is ±8%, based on repeated measurements of the same sample. International intercomparison exercises [*Putaud et al.*, 2000] showed that the overall uncertainties of TC (TC = OC + BC) and black carbon determinations are <10%, and ~40% for TC and BC, respectively.

[13] In the following calculation, instead of (OC), we will consider the particulate organic matter (POM), which includes, in addition to carbon, hydrogen atoms, and minor amounts of other species. The mass of particulate organic matter is computed from the mass of organic carbon as follows [*Liousse et al.*, 1996]:

$$\mathrm{POM} = 1.3 \times \mathrm{OC}. \quad (1)$$

[14] Na^+, NH_4^+, K^+, Mg^{2+}, Ca^{2+}, Cl^-, NO_3^-, and SO_4^{2-} concentrations were measured by ion chromatography. The uncertainty of the analyses was ±10% for all species [*Putaud et al.*, 2000]. Non-sea-salt sulfate fraction (e.g., $nssSO_4^{2-}$) was derived using Na^+ as a sea salt tracer and a standard sea salt composition. Ammonium sulfate (AS) concentration was computed using the $nssSO_4^{2-}$ fraction associated with the ammonium NH_4^+. Nitrate (N) was deduced from the NO_3^- concentrations. Sea salt (SS) concentrations were calculated from the Na^+ concentrations, the ratio of K^+, Mg^{2+}, Ca^{2+} and SO_{2-}^4 over Na^+ in standard seawater and the measured Cl^- concentrations to account for possible Cl^- depletion. Dust (D) concentrations were estimated from the amount of non sea salt Ca^{2+} measured in each impactor stage and the regression between non sea salt Ca^{2+} and ash (considered as mineral dust) determined from colocated and simultaneous sampling on Whatman 41 ashless filters. All these analyses are made on each impactor stage, allowing us to obtain in a first time, the mass size distribution of each component and in a second time, the total mass concentration of each component (noted M_i) by summing the concentrations of each stage.

3.2. Aerosol Optical Measurements

[15] In order to estimate the single scattering albedo from optical measurements, we used a CE 318 automatic sun tracking photometer (manufactured by CIMEL Electronique, Paris), which was part of the Aerosol Robotic Network (AERONET), which is an optical ground-based aerosol monitoring network and data archive supported by NASA's Earth Observing System and expanded by federation with many non-NASA institutions. The network hardware consists of identical automatic Sun-sky scanning spectral radiometers owned by national agencies and universities. Data from this collaboration provides globally distributed near real time observations of aerosol spectral optical depths, aerosol size distributions, and precipitable water in diverse aerosol regimes.

[16] The 318 automatic Sun-tracking photometer performed sky radiance and direct solar irradiance measurements over Marseille at 440, 670, 870, and 1020 nm wavelengths. AERONET observations have been shown capable to detect important variations of both magnitude and spectral dependence of ω_o that are consistent with aerosol type and emission conditions [*Dubovik et al.*, 2002]. The AERONET retrievals relies on *Dubovik and King* [2000] inversion algorithm deriving the single scattering albedo ($\omega_{o,aer}$) for the whole atmospheric column. The single scattering albedo retrieved by AERONET is valid for observed aerosol independently if it is internally or externally mixed. As shown in the *Dubovik et al.* [2000] paper, the retrieval gives the "optically equivalent" model of homogeneous particles with right single scattering albedo independently on particle mixing.

[17] The accuracy of individual aerosol properties retrieval by the *Dubovik and King* [2000] method from the measurements of CIMEL radiometers (performed under AERONET- standardized protocol of instrument maintenance and data processing) was analyzed in extensive sensitivity simulations [*Dubovik et al.*, 2000]. The analysis showed that an accurate ω_o retrieval (with accuracy to the level of 0.03) can be estimated for high aerosol loading (δ_a (440) $\geq$ 0.4) and for solar zenith angle $\geq$50° (the range of scattering angles in measured solar almucantar > 100°). For observations with lower aerosol loading, the retrieval accuracy of $\omega_{o,aer}$ decreases because of a decreasing of the information content. *Dubovik et al.*

Table 1. Aerosol Density $\rho_{(h)}$ (g cm^{-3}) at Ambient Humidity for Each Hydrophilic Aerosol Species

Date	h, %	$\rho_{(H)}^{SS}$	$\rho_{(H)}^{POM}$	$\rho_{(H)}^{AS}$ and $\rho_{(H)}^{N}$
23/06	37.50	1.740	1.353	1.471
24/06	61.40	1.487	1.246	1.313
25/06	61.00	1.636	1.247	1.206
26/06	45.00	1.636	1.310	1.406
02/07	45.00	1.608	1.297	1.387
03/07	55.00	1.608	1.319	1.387
04/07	50.00	1.608	1.297	1.387
10/07	71.50	1.371	1.297	1.236
11/07	42.00	1.612	1.299	1.389

[2000] have shown that for δ_a (440) $\leq$ 0.2, the accuracy levels drop down to 0.05–0.07 for $\omega_{o,aer}$ at 440 nm.

[18] During ESCOMPTE, 6 days (24, 25, and 26 June and 2, 3, and 4 July) agree with these conditions (δ_a (440) $\geq$ 0.4) and allowed us to compare the single scattering albedo retrieved by AERONET and computed from in-situ measurements at 550 nm. The AERONET retrieval are made at 440 and 670 nm for short wavelength, hence the values at 550 nm have been computed using a polynomial interpolation between the two values.

4. Method

[19] We present below the methodology we used to estimate the single scattering albedo of the total aerosol population for the two mixing state (external (section 4.1) and internal (section 4.2)). Our computations from the in situ measurements are based on the *Mie* [1908] theory, which allows deriving ω_o from the number size distribution (see sections 4.1.2 and 4.2.1) and the refractive index (see sections 4.1.3 and 4.2.2) of particles.

4.1. External Mixture

4.1.1. Aerosol Mass Size Distribution

[20] Concerning the external mixing state, all the aerosol particles (ammonium sulfate, nitrate, particulate organic matter, black carbon, sea salt, and dust) are investigated independently. The aerosol mass size distribution of each aerosol species is deduced from the in situ impactor measurements after some corrections. According to *Willeke and Baron* [1993], the impactor aerodynamic diameters, d_{ae}, were converted to geometric diameters, d_p, for each bin size, from the following relation:

$$d_p = d_{ae} \Big/ \sqrt{\rho_{(h)} C_{c,ae} \Big/ \rho_o C_{c,p}}, \quad (2)$$

where ρ_o = 1 g cm^{-3} and $C_{c,ae}$ and $C_{c,p}$ are the Cunningham slip correction factors for d_{ae} and d_p, respectively. Here $\rho_{(h)}$ is the aerosol density at ambient humidity computed by the formula:

$$\rho_{(h)} = \left(\rho_{(o)} + \left(GF_{(h)}^3 - 1\right)\rho_{(w)}\right)/GF_{(h)}^3, \quad (3)$$

where $\rho_{(o)}$ is the aerosol density in dry state, $\rho_{(w)}$ is the density of water (=1.0), and GF_a is the aerosol growth factor at ambient humidity computed from the *Hänel* [1976] relations. Here $\rho_{(h)}$ is only computed (Table 1) for the hydrophilic aerosol species as ammonium sulfate (AS), nitrate (N), and particulate organic matter (POM). Black carbon (BC) and dust aerosols (D) are considered as hydrophobic, and their density is not sensitive to humidity.

[21] In dry state, the aerosol density of 1.7 g cm^{-3} has been taken from *Sloane* [1984] for ammonium sulfate and nitrate, 2.1 g cm^{-3} for sea salt [*D'Almeida et al.*, 1991], 1.5 g cm^{-3} for particulate organic matter and black carbon (*Horvath* [1993] and *Chazette and Liousse* [2001], respectively), and 2.3 g.cm^{-3} for mineral aerosol.

[22] The aerosol mass size distribution (dM/dlogr) deduced from the concentrations measured on each impactor stage was then fitted with a lognormal function (the relation in equation (4)) (accounting for the respective collection efficiencies of the different cascade impactor stages), from which the parameters of the mass size distribution were retrieved, as the mass mode radius ($r_{g,m(i)}$) and the standard deviation (σ_i) of each component (i):

$$\frac{dM}{d\log r} = \sum_{i=1}^{n} \frac{M_i}{\sqrt{2\pi}\log\sigma_i} \exp\left[-\frac{1}{2}\left(\frac{\log r - \log r_{g,m(i)}}{\log\sigma_i}\right)^2\right]. \quad (4)$$

4.1.2. Aerosol Number Size Distribution

[23] The mass size distribution obtained by cascade impactor is elemental mass size distribution but can be easily transformed into number size distribution (dN/dlogr) (necessary for the Mie model input). Hence the particles were assumed to be spherical, and the "mass" distribution parameters ($r_{g,m(i)}$, σ_i, M_i) were transformed into "number" distribution parameters ($r_{g,n(i)}$, σ_i, N_i), corresponding to a number size distribution:

$$\frac{dN}{d\log r} = \sum_{i=1}^{n} \frac{N_i}{\sqrt{2\pi}\log\sigma_i} \exp\left[-\frac{1}{2}\left(\frac{\log r - \log r_{g,n(i)}}{\log\sigma_i}\right)^2\right], \quad (5)$$

where $r_{g,n(i)}$ and N_i are the number mode radius and the concentrations of particles (#.cm^{-3}) of each component (i), computed according to *Seinfeld and Pandis* [1998] relations:

$$\log\left(r_{g,n(i)}\right) = \log\left(r_{g,m(i)}\right) - 3(\log\sigma_i)^2 \ln 10 \quad (6)$$

$$N_i = 3M_i/4\pi\overline{r_i^3}\rho_{i(h)} \quad (7)$$

$$\overline{r_i^3} = r_{g,n(i)}^3\left(\frac{9}{2} \times \ln^2\sigma_i\right). \quad (8)$$

[24] The geometric standard deviation remains the same for the two distributions. In the relation in equation (7), M_i and $\rho_{i(h)}$ are the mass concentration and the particulate density at ambient humidity of the component (i) (Table 1), respectively, while $\overline{r_i}$ is the equivalent radius (the relation in equation (8)). All the results of the lognormal function characteristics for the number size distributions are given by *Mallet et al.* [2003] and summarized in Table 2 for the entire aerosol species studied. It should be noted that the accumulation and the coarse modes of a mass size distribution correspond, after transformation, to the fine

Table 2. Aerosol Microphysical Properties ($r_{g,n(o)}$, $r_{g,n(h)}$, σ, N) for Each Aerosol Species

Aerosol	Mode		23/06	24/06	25/06	26/06	02/07	03/07	04/07	10/07	11/07	Mean
BC	Fine	$r_{g,n}$	0.017	0.046	0.025	0.019	0.039	0.031	0.037	0.020	0.027	0.028 ± 0.010
		σ	2.07	1.71	1.97	2.03	1.77	1.85	1.82	2.15	1.95	1.94 ± 0.14
		N	3632	675	2731	5170	2156	918	470	2171	954	-
POM	Fine	$r_{g,n(o)}$	0.026	0.036	0.016	0.023	0.015	0.024	0.025	0.042	0.037	0.027 ± 0.010
		$r_{g,n(h)}$	0.029	0.046	0.023	0.027	0.018	0.029	0.031	0.057	0.044	0.034 ± 0.010
		σ	1.76	1.77	2.06	1.98	2.17	1.85	1.82	1.78	1.65	1.86 ± 0.16
		N	6012	1970	8524	7256	8330	5737	4003	710	2003	-
	Accumulation	$r_{g,n(o)}$	0.310	0.223	0.192	0.404	0.437	0.197	0.145	0.305	0.408	0.291 ± 0.100
		$r_{g,n(h)}$	0.330	0.282	0.275	0.473	0.534	0.241	0.177	0.410	0.484	0.364 ± 0.120
		σ	1.90	1.98	2.18	1.84	1.66	2.17	2.20	1.87	1.76	1.95 ± 0.19
		N	0.933	1.29	1.31	0.69	0.612	1.439	2.34	0.87	0.66	-
AS	Fine	$r_{g,n(o)}$	0.034	0.046	0.037	0.034	0.039	0.045	0.048	0.044	0.047	0.040 ± 0.005
		$r_{g,n(h)}$	0.039	0.060	0.048	0.041	0.046	0.056	0.058	0.063	0.055	0.050 ± 0.010
		σ	1.76	1.65	1.78	1.84	1.69	1.63	1.66	1.68	1.78	1.74 ± 0.07
		N	4700	3926	3688	4960	4600	2981	2344	3608	1182	-
N	Accumulation	$r_{g,n(o)}$	0.520	0.508	0.502	0.526	0.518	0.481	0.505	0.463	0.530	0.505 ± 0.020
		$r_{g,n(h)}$	0.595	0.664	0.657	0.624	0.614	0.604	0.616	0.659	0.619	0.628 ± 0.030
		σ	1.62	1.60	1.61	1.64	1.66	1.68	1.57	1.62	1.51	1.61 ± 0.05
		N	0.4	0.68	0.29	0.32	0.31	0.24	0.34	0.48	0.19	-
SS	Accumulation	$r_{g,n(o)}$	0.451	0.340	0.316	0.355	0.314	0.398	0.343	0.285	0.409	0.350 ± 0.050
		$r_{g,n(h)}$	0.515	0.440	0.413	0.421	0.372	0.500	0.418	0.405	0.478	0.440 ± 0.030
		σ	1.69	1.77	1.74	1.78	1.83	1.72	1.75	1.81	1.73	1.75 ± 0.04
		N	0.34	0.81	0.27	0.45	0.41	0.12	0.42	0.67	0.71	-
Dust	Fine	$r_{g,n}$	0.044	0.044	0.011	0.018	0.017	0.030	0.079	0.044	-	0.036 ± 0.010
		σ	2.27	1.57	2.40	2.18	2.15	2.00	1.56	1.67	-	1.97 ± 0.3
		N	180	236	4730	1871	1544	426	225	420	514	-
	Accumulation	$r_{g,n}$	0.554	0.596	0.163	0.365	0.376	0.319	0.264	0.363	-	0.360 ± 0.130
		σ	1.73	1.68	2.37	1.95	1.94	2.06	2.03	1.92	-	1.98 ± 0.21
		N	0.153	0.17	6.11	1.89	0.94	2.38	1.436	1.76	0.57	-

and the accumulation modes, respectively, of a classical number size distribution [*Whitby*, 1978].

4.1.3. Refractive Index

[25] The complex refractive index is required to compute, associated with the characteristics of the lognormal number aerosol size distribution, the aerosol optical properties. This refractive index depends on the chemical nature of the particle and consists of a real part n and an imaginary part, k.

[26] In the case of an external mixture, we compute the complex refractive index for each component noted $m_{i(h)}$ ($m_{i(h)} = n_{i(h)} - ik_{i(h)}$) at the ambient humidity (h) (reported in Table 3 for hydrophilic aerosol), from the *Hänel* [1976] relations at wavelength λ:

$$m_{i(h)}(\lambda) = m_{h2o}(\lambda) + \left(m_{i(o)}(\lambda) - m_{h2o}(\lambda)\right)\left(\frac{r_{g,n(i)(h)}}{r_{g,n(i)(o)}}\right)^{-3}, \quad (9)$$

where m_{h2o} is the pure water refractive index and $m_{i(o)}$ the refractive index of the aerosol species (i) in dry state and generally referenced in literature.

[27] At 550 nm and in dry state, the refractive index of 1.55−0.005i has been taken from *Von Hoyningen-Huene et al.* [1998] for particulate organic matter. The refractive index used for ammonium sulphate, sea salt and dust have been taken from *D'Almeida et al.* [1991], with values equals to $1.53\text{-}6.00e^{-3}i$, $1.38\text{-}4.26^{e\text{-}9}i$, and $1.53\text{-}5.50e^{-3}i$, respectively. Finally, the value of 1.85-0.56i has been taken for black carbon particles from a recent study of *Marley et al.* [2001].

[28] The number mode radius in dry state $r_{g,n(o)}$ and at ambient humidity $r_{g,n(h)}$, are linked by the relation:

$$r_{g,n(o)} = r_{g,n(h)}(1-h)^{e}, \quad (10)$$

where h is the relative humidity. The coefficient e depends on the considered type of aerosol. It is equal to 0.25 for particulate organic matter [*Chazette and Liousse*, 2001], to 0.285 for ammonium sulfate, nitrate, and sea salt [*Hänel*, 1976], and e = 0 for black carbon and dust assumed to be nonhygroscopic.

[29] From the microphysical properties ($r_{g,n(i)(h)}$, σ_i, N_i, $m_{i(h)}$, (λ)) obtained for each component (i), we computed (Table 4) its optical properties at different wavelengths (440, 550, 670, 870, and 1020 nm). We focused here the optical computations on the extinction coefficient $K_{ext(i)}$ and the single scattering albedo $\omega_{o(i)}$ necessary to compute $\omega_{o,ext}$ in the external mixture case, for the total aerosol population, as follows:

$$\omega_{o,ext} = \frac{\sum_i K_{ext(i)} \times \omega_{o(i)}}{\sum_i K_{ext(i)}} \quad (11)$$

4.2. Internal Mixture

4.2.1. Aerosol Mass and Number Size Distribution

[30] In the case of the internal mixture, all the aerosol species are used to estimate the aerosol number size distribution. As it was the case for the external mixture,

Table 3. Aerosol Refractive Index, m_h ($m_h = n - ik$) at 550 nm, in Wet State

Date	h, %	$n_{(SS)}$	$k_{(SS)}$	$n_{(POM)}$	$k_{(POM)}$	$n_{(AS\&N)}$	$k_{(AS\&N)}$
23/06	37.5	1.444	7.38 e-9	1.438	0.0035	1.466	0.0040
24/06	61.4	1.402	5.54 e-9	1.440	0.0024	1.421	0.0027
25/06	61.0	1.407	5.55 e-9	1.440	0.0025	1.421	0.0027
26/06	45.0	1.426	6.63 e-9	1.466	0.0031	1.447	0.0035
02/07	45.0	1.423	6.40 e-9	1.460	0.0030	1.442	0.0033
03/07	55.0	1.423	6.40 e-9	1.471	0.0032	1.440	0.0030
04/07	50.0	1.423	6.40 e-9	1.460	0.0030	1.441	0.0031
10/07	71.5	1.388	4.75 e-9	1.416	0.0020	1.400	0.0021
11/07	42.0	1.438	7.00 e-9	1.477	0.0033	1.456	0.0038

Table 4. Optical Properties ($K_{ext,i}$ and $\omega_{o,i}$) of Each Aerosol Species i at 550 nm and in Wet State

Aerosol	Mode		23/06	24/06	25/06	26/06	02/07	03/07	04/07	10/07	11/07	mean
BC	Fine	K_{ext}	0.010	0.015	0.018	0.017	0.010	0.008	0.006	0.012	0.007	0.012 ± 0.004
		ω_o	0.31	0.37	0.34	0.31	0.29	0.34	0.36	0.35	0.35	0.33 ± 0.03
POM	Fine	K_{ext}	0.005	0.011	0.012	0.017	0.009	0.008	0.006	0.010	0.006	0.009 ± 0.004
		ω_o	0.96	0.98	0.98	0.97	0.97	0.97	0.97	0.98	0.97	0.98 ± 0.01
	Accumulation	K_{ext}	0.002	0.002	0.003	0.003	0.002	0.002	0.002	0.003	0.001	0.002 ± 0.001
		ω_o	0.95	0.96	0.95	0.93	0.94	0.94	0.95	0.96	0.93	0.94 ± 0.01
AS	Fine	K_{ext}	0.015	0.038	0.027	0.028	0.021	0.019	0.023	0.043	0.019	0.026 ± 0.010
		ω_o	0.96	0.98	0.98	0.97	0.97	0.97	0.97	0.98	0.97	0.97 ± 0.005
N	Accumulation	K_{ext}	0.001	0.004	0.001	0.001	0.001	0.001	0.001	0.002	0.001	0.002 ± 0.001
		ω_o	0.91	0.94	0.94	0.92	0.92	0.92	0.93	0.95	0.92	0.93 ± 0.01
SS	Accumulation	K_{ext}	0.001	0.002	0.0001	0.001	0.001	0.0004	0.001	0.002	0.002	0.0010 ± 0.0007
		ω_o	0.99	0.99	0.99	0.99	0.99	0.99	0.99	0.99	0.99	0.99 ± 0.001
Dust	Fine	K_{ext}	0.0004	0.0005	0.0032	0.0032	0.0017	0.0021	0.00025	0.0018	0.0016	0.0016 ± 0.0011
		ω_o	0.96	0.96	0.96	0.96	0.96	0.96	0.96	0.96	0.96	0.96 ± 0.02
	Accumulation	K_{ext}	0.0006	0.0008	0.0059	0.0049	0.0026	0.0055	0.0022	0.0044	0.0013	0.0031 ± 0.0020
		ω_o	0.88	0.88	0.90	0.89	0.89	0.89	0.91	0.90	0.90	0.89 ± 0.01

the impactor aerodynamic diameters d_{ae} were converted to geometric diameters, d_p, for each bin size according to the *Willeke and Baron* [1993] relations (see the relation in equation (2)). We computed in this case the equivalent aerosol density $\overline{\rho_{(h)}}$ at ambient relative humidity as follows:

$$\overline{\rho_{(h)}} = \sum_i \rho_{i(h)} \times f_i, \tag{12}$$

where $\rho_{i(h)}$ (Table 1) and f_i are the aerosol density and the volume fraction of the component (i), (computed from the mass of the component M_i and the aerosol density $\rho_{i(h)}$), respectively.

[31] Then, in the same way than for the external mixture, the aerosol mass size distributions deduced from concentrations measured on each impactor stage (Figure 2), which present a bimodal structure, were fitted with a lognormal function from which the mass mode radius ($r_{g,m}$), the standard deviation (σ) and the associated "number" parameters ($r_{g,n}$, σ, N) were retrieved. Values of the lognormal parameters, for the number size distribution and for the fine and the accumulation mode are reported Table 5.

4.2.2. Refractive Index

[32] Different mixing rules exist to estimate the complex refractive index in the internal mixture state. Recently, the volume average, Maxwell-Garnett, and Bruggeman mixing rules have been tested for typical atmospheric aerosols by *Lesins et al.* [2002]. Results indicated that the refractive index was insensitive to the choice of the mixing rule and the effect on the optical properties was less than 1%. Hence the simple volume average procedure is used in this study to estimate the mean refractive index for each mode (fine and accumulation). The real and imaginary parts of the refractive index noted $\overline{n_h}$ and $\overline{k_h}$ are determined by the volume average procedure as following:

$$\begin{aligned} \overline{n_h} &= \sum_{i=1}^{n} n_{i(h)} f_i \\ \overline{k_h} &= \sum_{i=1}^{n} k_{i(h)} f_i, \end{aligned} \tag{13}$$

where $n_{i(h)}$ and $k_{i(h)}$ are the real and the imaginary part of the refractive index of each component (i) at ambient relative humidity (Table 3), respectively, and f_i is the volume

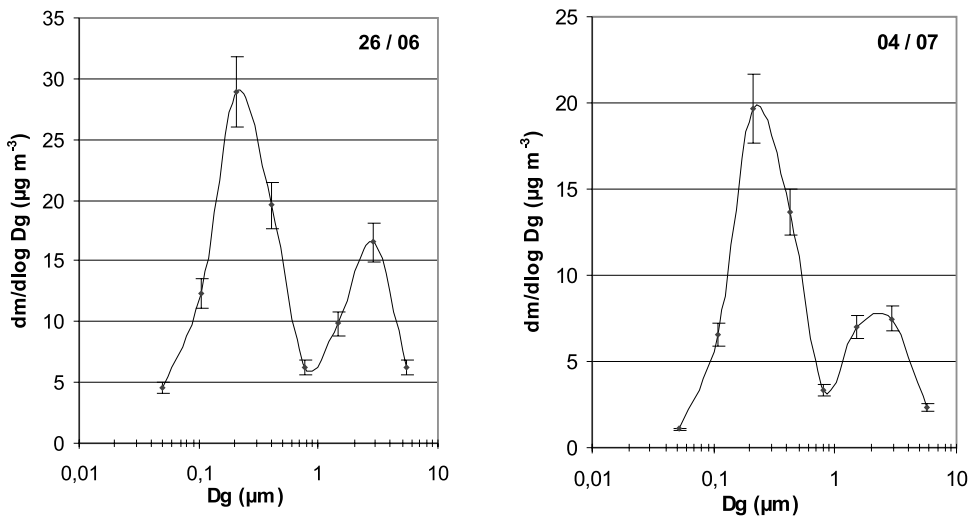

Figure 2. Two examples (26 June and 4 July) of aerosol mass size distributions in internal mixture state measured during IOPs. See color version of this figure in the HTML.

Table 5. Aerosol Microphysical Properties of the Log-Normal Number Size Distribution in the Internal Mixture Case (f and a Stand for the Fine Mode and the Accumulation Mode, Respectively)

	23/06	24/06	25/06	26/06	02/07	03/07	04/07	10/07	11/07
$r^{f}_{g,n(h)}/\sigma$	0.024/1.94	0.042/1.79	0.030/2.02	0.026/2.01	0.034/1.84	0.040/1.77	0.046/1.77	0.066/1.67	0.025/2.08
$r^{a}_{g,n(h)}/\sigma$	0.45/1.80	0.58/1.63	0.49/1.82	0.709/1.67	0.709/1.70	0.45/1.84	0.52/1.67	0.56/1.67	0.678/1.58

fraction of the component (i). Values estimated for each day for the fine (f) and the accumulation (a) mode are reported Table 6. The imaginary part of the refractive index, k (which describes the absorptivity of a material) is comprised between 0.032 and 0.062 for the fine mode, depending on the mass fraction of black carbon. The characteristics of the number size distribution (Table 5), associated with the refractive index of each mode (Table 6) are used in the Mie theory to compute the single scattering albedo ($\omega_{o,int}$) in the internal mixture state for the total aerosol population.

4.3. Sensitivity Tests

[33] Table 7 indicates sensitivity tests focused on the single scattering albedo for the two mixing states. These optical computations are based on the variation of the parameters required in the Mie theory and used to compute the single scattering albedo. The optical computations have been made at 550 nm.

[34] We first start the sensitivity test by computing errors due to the uncertainty on the concentration of the scattering aerosol and especially ammonium sulfate, assuming ±20% on the retrieval mass. We obtained an error bar on the single scattering albedo equal to ±0.011 and ±0.013 for the external and internal mixing, respectively. Then, we focused on the uncertainty due to the black carbon aerosol, which is the major contributor to absorption [*Mallet et al.*, 2003].

[35] In the external mixture case, we considered first uncertainties in the shape of the black carbon size distribution, ($\Delta m_{(BC)}$ = ±25%, $\Delta r_{g,m(BC)}$ = ±10%, and $\Delta\sigma_{(BC)}$ = ±10%). Second, we considered uncertainty on the imaginary (between 0.45 and 0.70) and the real (between 1.75 and 1.95) parts of the black carbon refractive index, corresponding to an aged and a value close to a pure black carbon aerosol, respectively. Finally, we considered uncertainty on the black carbon aerosol density ($\Delta\rho_{BC}$ = ±25%).

[36] In the internal mixture case, we considered in a first time uncertainties in the shape of the total number size distribution presented in section 4.2.1, ($\Delta r_{g,m}$ = ±10%, $\Delta\sigma$ = ±10%). In a second time, we considered the same uncertainties on the black carbon refractive index, density ($\Delta\rho_{BC}$ = ±25%) and black carbon mass ($\Delta m_{(BC)}$ = ±25%) used for the external mixture case.

[37] Concerning the external mixture, the results presented Table 7 indicated an error bar on ω_o comprised between ±0.010 (corresponding to the uncertainty on the black carbon aerosol density, $\rho_{(BC)}$) and ±0.017 (corresponding to the uncertainty on the black carbon mass, $m_{(BC)}$). The error on ω_o due to the uncertainty on the black carbon refractive index value is equal to ±0.010, and the error due to the uncertainty on the shape of the black carbon size distribution is equal to ±0.003 (for $r_{g,m(BC)}$) and ±0.003 (for $\sigma_{(BC)}$).

[38] Concerning the internal mixture case, optical simulations indicate an error bar on ω_o comprised between ±0.001 (corresponding to the uncertainty on the value of the standard deviation of the total number size distribution (see section 4.2.1)) and ±0.026 (corresponding to the uncertainty on the value of the black carbon refractive index).

[39] In these two mixing cases, it should be noted that most of the error sources are correlated each others and we could then reasonably estimate an error bar equal to ±0.04 at 550 nm for $\omega_{o,int.}$ and $\omega_{o,ext.}$. This error bar is relevant compared to the variation of the single scattering albedo between the two mixing cases and the Aeronet retrieval accuracy.

5. Results and Discussion

5.1. External and Internal Single Scattering Albedo

[40] The values of the single scattering albedo obtained for the two mixing states are presented Figure 3 (for 26 June and 4 July) at different wavelengths (440, 550, 670, 870, and 1020 nm). The single scattering albedo is found to be sensitive to the mixing state. Indeed, $\omega_{o,ext}$ is comprised between 0.79 and 0.88 at 550 nm in wet state with a mean value of 0.85 ± 0.04, while $\omega_{o,int}$ is comprised between 0.70 and 0.82 with a mean value equal to 0.75 ± 0.04.

[41] We note the same tendency at different wavelengths as shown Figure 3. For all the days studied, the single scattering albedo in the internal mixture case is found to be 15% lower than for the external mixture case. This probably leads to an increase of the solar radiation absorption into the atmospheric layer. This result is in a rather good agreement with simulations realized by *Lesins et al.* [2002], which indicated that the dry single scattering albedo (for the case of a black carbon mass fraction of 0.1) could be reduced by 22% in the internal mixture case.

[42] This diminution of the single scattering albedo could be explained by the fact that in the external mixture state, all the absorption is concentrated in the pure black carbon particles, while in the internal mixture, the absorbing component is spread over all particles. The absorption cross section of a given amount of black carbon in a particle that consists also of nonabsorbing material is

Table 6. Mean Refractive Index of the Fine and the Accumulation Modes at 550 nm in Wet State for the Internal Mixture Case

	23/06	24/06	25/06	26/06	02/07	03/07	04/07	10/07	11/07
$\overline{m_f}$	1.503-0.052i	1.456-0.042i	1.504-0.062i	1.496-0.057i	1.481-0.043i	1.481-0.039i	1.470-0.034i	1.486-0.032i	1.491-0.040i
$\overline{m_a}$	1.472-0.004i	1.423-0.003i	1.508-0.007i	1.497-0.010i	1.487-0.006i	1.487-0.004i	1.482-0.010i	1.537-0.009i	1.482-0.016i

Table 7. Errors Bars on the Single Scattering Albedo at 550 nm, for the External and Internal Mixing States, in Function of the Variation of the Main Required Parameters for the Mie Theory[a]

	$\Delta\omega_{o(ext.)}$	$\Delta\omega_{o(int.)}$
$\Delta m_{(AS)}$	±0.011	±0.013
$\Delta m_{(BC)}$	±0.017	±0.021
$\Delta r_{g,m(BC)}$	±0.003	#
$\Delta\sigma_{(BC)}$	±0.003	#
$\Delta r_{g,m}$	#	±0.010
$\Delta\sigma$	#	±0.001
$\Delta m_{(BC)}$	±0.010	±0.026
$\Delta\rho_{(BC)}$	±0.015	±0.025

[a]Variations used for the input parameters and presented in detail in the text.

greater than that of the pure black carbon particle in air. Hence in the internal mixture, the black carbon exerts its influence in the absorption of every single particle, which exceeds that if all the black carbon is concentrated exclusively in pure black carbon particles as described by *Seinfeld and Pandis* [1998].

[43] This first step confirms that the single scattering albedo represents an interesting tool in order to retrieve information about the mixing state of black carbon with other aerosol species. As it was mentioned in the introduction, the second step consists to compare ω_o deduced from our in situ measurements with ω_o values provided by an independent optical measurement, here the ω_o AERONET retrieval sun photometer [*Dubovik et al.*, 2000].

5.2. Comparisons With AERONET Retrieval

[44] The ESCOMPTE experiment, in the contrary of TARFOX [*Russell et al.*, 1999] or INDOEX [*Ramanathan et al.*, 2001], was not dedicated to the study of the direct radiative impact of aerosol. Hence few optical measurements have been performed during this experiment. The only independent optical measurements were performed by the Sun-photometer instrument (see section 3.2) during the different IOPs studied here. However, in order to compare the single scattering albedo deduced from the in situ measurements with the one inverted by the photometer, we had to study the aerosol vertical repartitions to investigate the representivity of our measurements made in situ, near ground level, with information concerning the total atmospheric column, deduced from the CIMEL photometer.

[45] During the ESCOMPTE experiment, the aerosol concentrations profiles recorded during the ARAT aircraft flights [*Van Dingenen et al.*, 2002a, 2002b] indicated that aerosols were mainly confined in the PBL which is close to 1 km, as shown Figure 4. Records of the potential temperature profiles (Figure 4), show, for all the days studied, a positive gradient, indicating a stable and well-homogenized PBL. Furthermore, the *Angström* [1964] coefficient $\alpha_{440/670}$ is comprised between 1.10 and 1.82 for all the days studied. This implies that the extinction is mainly due to submicronic anthropogenic aerosol [*Liousse et al.*, 1995] and shows just that no dust events were observed during the days studied in this work. Hence we assumed that the ground-based aerosol optical characterization was representative of the whole aerosol layer mainly confined in the PBL, and might be compared with the AERONET retrievals.

[46] Comparisons at 550 nm (in wet state) of $\omega_{o,int}$, $\omega_{o,ext}$, and $\omega_{o,aer}$ are reported Figure 5. We noted clearly a relatively good agreement between $\omega_{o,ext}$ and $\omega_{o,aer}$, where the different values are very close and comprised into the error bars for each day studied. In the contrary, the values of ω_o inverted by AERONET and those computed in the case of an internal mixture are outside of the error bars of the two approaches. This seems to indicate that the black carbon aerosol is probably mixed in external mixture with other aerosol species on the Vallon d'Ol urban site.

[47] This important result is coherent with numerous other studies. Indeed, *Jacobson* [2001] estimated that 5 days are needed to particles of pure black carbon, after entering the atmosphere, to end up in mixtures containing dust, sea spray, sulphate, and other chemicals. Furthermore, this result is coherent with in situ observations from previous study by *Covert and Heintzenberg* [1984], which indicated a large degree of external mixture of particles in urban zone. More recently, *Hasegawa and Ohta* [2002] reported that only 5–7% of internally mixed black carbon was observed in urban site (Sapporo city, Japan). The same conclusion is again observed by *Van Dingenen et al.* [2002a, 2002b], which reported strong differences in mixing state between urban background (mostly externally mixed) and rural

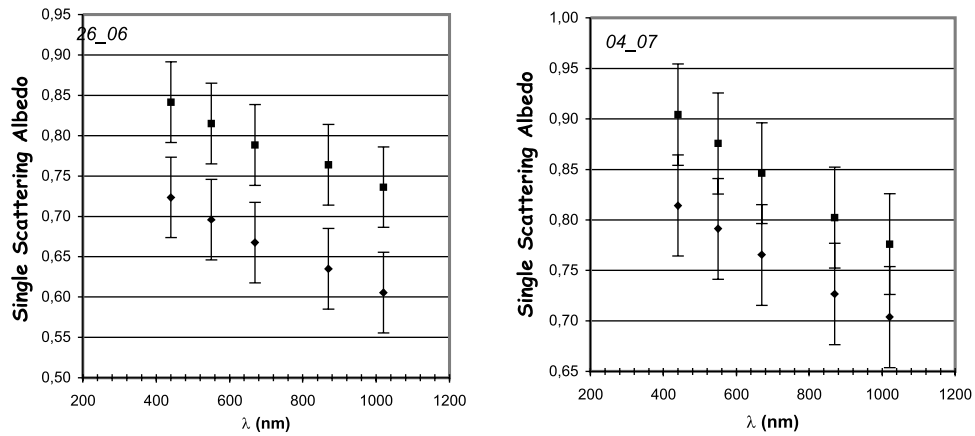

Figure 3. Two examples (26 June and 4 July) of $\omega_o(\lambda)$ at different wavelengths for the two mixing state (internal, indicated by diamond, and external, indicated by square).

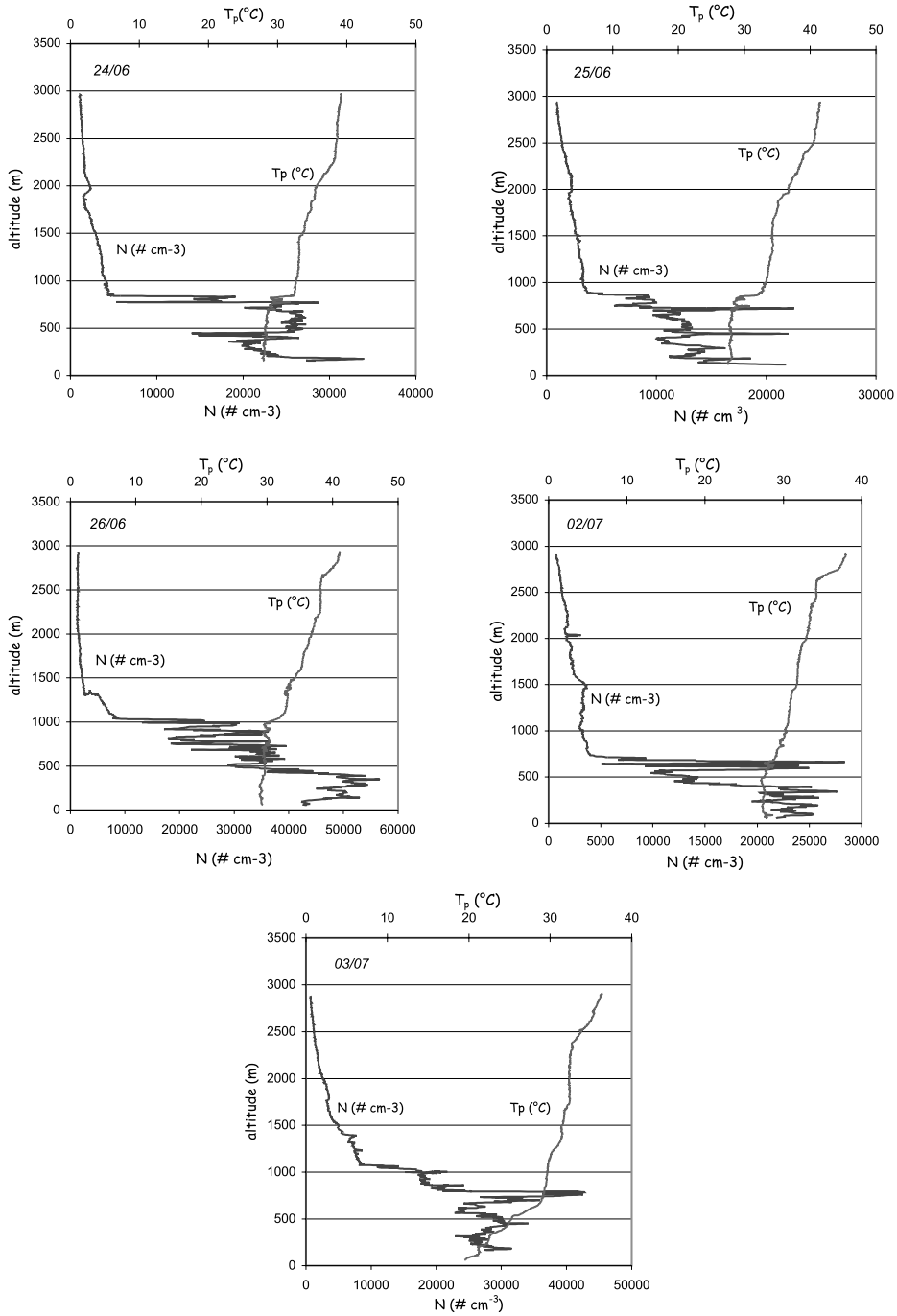

Figure 4. Number concentrations and potential temperature profiles. See color version of this figure in the HTML.

(mostly internally mixed). Hence the freshly emitted black carbon should be usually hydrophobic and externally mixed with other aerosol species.

[48] This clearly indicates the interest of this study, which provides crucial information on the mixing state of black carbon aerosol. It could duplicate any experiments (TARFOX, INDOEX) as soon as the aerosol chemical composition and independent optical measurements are performed simultaneously. Nevertheless, in the case of atmospheric structure more complex than these observed during ESCOMPTE, as for example dust layer, the ω_o retrieval performed by the Sun-tracking photometer could be not representative of in situ ground based aerosol characterization. In this case, ground-based optical measurements, as nephelometer and aethalometer should be surely more representative of the air mass used to perform the aerosol chemical characterization.

6. Conclusion

[49] We have investigated the mixing state of black carbon particles with other aerosol species in urban zone

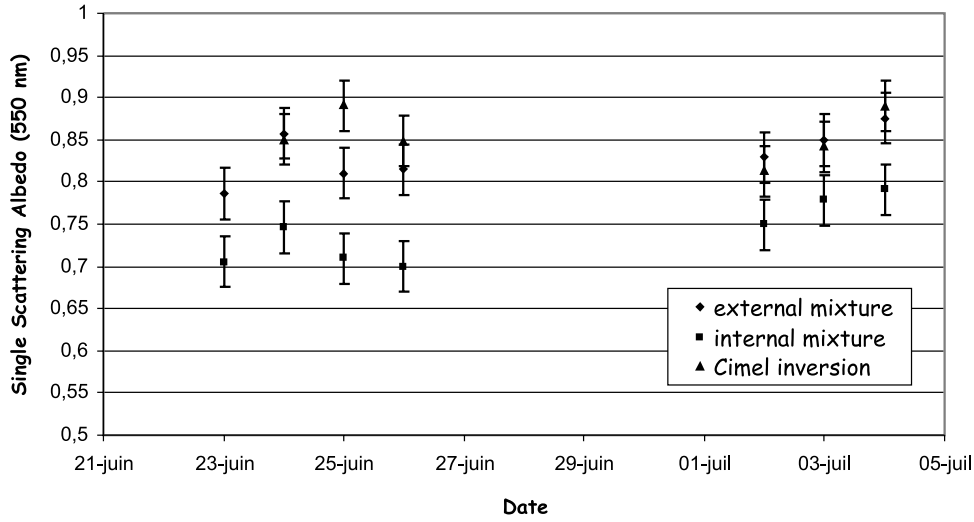

Figure 5. Comparisons of ω_o computed for the two mixing state with ω_o retrieved by AERONET at 550 nm. See color version of this figure in the HTML.

during the ESCOMPTE experiment conducted during summer of 2001 in France. The type of mixture was identified by comparison of ω_o simulated from in situ data for the two mixing state with the AERONET single scattering albedo values derived from Sun-photometer observation. For computing ω_o from in situ observations, we have employed Mie calculations with size distributions and refractive indices determined from ground-based chemical and microphysical measurements. The results of such computations, as expected according numerous publications [e.g., *Haywood and Shine*, 1995; *Lesins et al.*, 2002], show the large difference of simulated single scattering albedos for the two mixing state. Indeed, the single scattering albedo is found to be lower by as much as 15% in the internal mixture case ($\omega_{o,int} = 0.75 \pm 0.04$) than compared to the external mixture state ($\omega_{o,ext} = 0.85 \pm 0.04$). The mean values of single scattering albedo ($\omega_{o,aer} = 0.84 \pm 0.04$) provided by AERONET retrieval is found to be close to the in situ single scattering albedo obtained under assumption of external mixture. The same result was found in comparisons of individual in situ and AERONET $\omega_{o,aer}$ observed for all the days studied in this work. This agreement of remote sensing observations of single scattering albedo with in situ values constrained by the assumption of external coexistence of absorbing and nonabsorbing aerosol components suggests external mixing of black carbon with other species in the urban aerosol observed during ESCOMPTE measurement campaign. This finding is coherent with recent studies carried out in similar environment, indicating that close to the source of pollution, black carbon particles are mostly found to be externally mixed with other aerosol species.

[50] **Acknowledgments.** The authors are indebted to Hélène Cachier, Bernard Cros, and Pierre Durand for the organization of ESCOMPTE experiment. They gratefully thank the different Institutes in France (CNRS, INSU, PNCA, PRIMEQUAL, ADEME, and Ministry of Environment) for their support. Logistic help from local agencies (AIRMARAIX and AIRFOBEP) is gratefully acknowledged. We also thank the AERONET/PHOTONS staff for the data collection, calibration, and processing. We would also like to thank especially the AERONET/PHOTON PIs during ESCOMPTE: P. Goloub (LOA), L. Blarel (LOA), D. Bahaiddin (CIMEL), and D. Tanré (LOA).

References

Adams, P. J., J. H. Seinfield, D. Koch, L. Mickley, and D. Jacob (2001), General circulation model assessment of direct radiative forcing by the sulphate-nitrate-ammonium-water inorganic aerosol system, *J. Geophys. Res.*, *106*, 111–1097.

Ackerman, A. S., and O. S. Toon (1981), Absorption of visible radiation in atmosphere containing mixtures of absorbing and non absorbent particles, *Applied Optics*, *20*, 3661–3668.

Angström, A. (1964), The parameters of atmospheric turbidity, *Tellus*, *16*, 64–75.

Cachier, H., M.-P. Brémond, and P. Buat-Ménard (1989), Determination of atmospheric soot carbon with a simple thermal method, *Tellus, Ser. B*, *41*, 379–390.

Chazette, P., and C. Liousse (2001), A case study of optical and chemical ground apportionment for urban aerosols in Thessaloniki, *Atmos. Environ.*, *35*, 2497–2506.

Cooke, W. F., C. Liousse, H. Cachier, and J. Feichter (1999), Construction of a 1° × 1° fossil fuel emission data set for carbonaceous aerosol and implementation and radiative impact in the ECHAM4 model, *J. Geophys. Res.*, *104*, 22,137–22,162.

Covert, D. S., and J. Heintzenberg (1984), Measurements of the degree of internal/external mixing of hygroscopic compounds and soot in atmospheric aerosols, *Sci. Total Environ.*, *36*, 347–352.

Cros, B., et al. (2004), An overview of the ESCOMPTE Campaign, *Atmos. Res.*, in press.

D'Almeida, G. A., P. Koepke, and E. P. Shettle (1991), *Atmospheric Aerosols: Global Climatology and Radiative Characteristics*, 561 pp., A. Deepak, Hampton, Va.

Dubovik, O., and M. D. King (2000), A flexible inversion algorithm for retrieval of aerosol optical properties from Sun and sky radiance measurements, *J. Geophys. Res.*, *105*, 20,673–20,696.

Dubovik, O., A. Smirnov, B. N. Holben, M. D. King, Y. J. Kaufman, T. F. Eck, and I. Slutsker (2000), Accuracy assessments of aerosol optical properties retrieved from AERONET Sun and sky-radiance measurements, *J. Geophys. Res.*, *105*, 9791–9806.

Dubovik, O., B. N. Holben, T. F. Eck, A. Smirnov, Y. J. Kaufman, M. D. King, D. Tanré, and I. Slutsker (2002), Variability of absorption and optical properties of key aerosol types observed in worldwide locations, *J. Atmos. Sci.*, *59*, 590–608.

Hänel, G. (1976), The properties of atmospheric particles as functions of the relative humidity at thermodynamic equilibrium with surrounding moist air, *Adv. Geophys.*, *19*, 73–188.

Hasegawa, S., and S. Ohta (2002), Some measurements of the mixing state of soot-containing particles at urban and non-urban sites, *Atmos. Environ.*, *36*, 3899–3908.

Haywood, J. M., and V. Ramaswamy (1998), Global sensitivity studies of the direct radiative forcing due to anthropogenic sulphate and black carbon aerosols, *J. Geophys. Res.*, *103*, 6043–6058.

Haywood, J. M., and K. P. Shine (1995), The effect of anthropogenic sulfate and soot aerosol on the clear sky planetary radiation budget, *Geophys. Res. Lett.*, *22*, 603–606.

Haywood, J. M., D. L. Roberts, A. Slingo, J. M. Edwards, and K. P. Shine (1997), General circulation model calculations of the direct radiative forcing of tropospheric sulphate and fossil-fuel soot aerosol, *J. Clim.*, *10*, 1562–1577.

Hegg, A. D., J. Livingston, P. V. Hobbs, T. Novakov, and P. Russel (1997), Chemical apportionment of aerosol column optical depth off the mid-Atlantic coast of the United States, *J. Geophys. Res.*, *102*, 25,293–25,303.

Horvath, H. (1993), Atmospheric light absorption—A review, *Atmos. Environ., Part A*, *27*, 293–317.

Houghton, J. T., et al. (Eds.) (2001), *Climate Change*, Cambridge Univ. Press, New York.

Jacobson, M. Z. (2001), Strong radiative heating due to the mixing state of black carbon in atmospheric aerosols, *Nature*, *409*, 695–697.

Lesins, G., P. Chylek, and U. Lohmann (2002), A study of internal and external mixing scenarios and its effect on aerosol optical properties and direct radiative forcing, *J. Geophys. Res.*, *107*(D10), 4094, doi:10.1029/2001JD000973.

Liousse, C., C. Devaux, F. Dulac, and H. Cachier (1995), Aging of savanna biomass burning aerosols: Consequences of their optical properties, *J. Atmos. Chem.*, *22*, 1–17.

Liousse, C., J. E. Penner, C. Chuang, J. J. Walton, H. Eddleman, and H. Cachier (1996), A global three-dimensional model study of carbonaceous aerosols, *J. Geophys. Res.*, *101*, 19,411–19,432.

Mallet, M., J. C. Roger, S. Despiau, O. Dubovik, and J. P. Putaud (2003), Microphysical and optical properties of aerosol particles in urban zone during ESCOMPTE, *Atmos. Res.*, *69*(1–2), 73–97.

Marley, N. A., S. G. Gaffney, J. C. Baird, C. A. Blazer, P. J. Drayton, and J. E. Frederick (2001), An empirical method for the determination of the complex refractive index of size-fractionated atmospheric aerosols for radiative transfer calculations, *Aerosol Sci. Technol.*, *34*, 535–549.

Middlebrook, A. M., D. M. Murphy, and D. S. Thomson (1998), Observations of organic material in individual marine particles at Cape Grim during the First Aerosol Characterization Experiment (ACE 1), *J. Geophys. Res.*, *103*, 16,475–16,483.

Mie, G. (1908), Beiträge zur Optick trüber medien, speziell kolloidaler Metallösungen, *Ann. Phys. Leipzig*, *25*, 377–445.

Putaud, J. P., et al. (2000), Chemical mass closure and assessment of the origin of the submicron aerosol in the marine boundary layer and the free troposphere at Tenerife during ACE-2, *Tellus, Ser. B*, *52*, 141–168.

Ramanathan, V., et al. (2001), The Indian Experiment: An integrated assessment of the climate forcing and effects of the great indo-asian haze, *J. Geophys. Res.*, *106*, 28,371–28,398.

Russell, P. B., P. V. Hobbs, and L. L. Stowe (1999), Aerosol properties and radiative effects in the United States east coast haze plume: An overview of the Tropospheric Aerosol Radiative Forcing Observational Experiment (TARFOX), *J. Geophys. Res.*, *104*, 2289–2307.

Seinfeld, J. H., and S. N. Pandis (1998), From air pollution to climate change, in *Atmospheric Chemistry and Physics*, p. 126, John Wiley, New York.

Sloane, C. S. (1984), Optical properties of aerosols of mixed composition, *Atmos. Environ.*, *18*, 871–878.

Van Dingenen, R., J. P. Putaud, A. Dell'Acqua, J. Viidanoja, S. Martins-Dos Santis, D. Roselli, and F. Raes (2002a), Hygroscopic properties of sub-micrometer aerosols in different smog regimes, paper presented at IGAC Conf., Heraklion, Crete.

Van Dingenen, R., J. P. Putaud, A. Dell'Acqua, S. Martins-Dos Santis, J. Viidanoja, and F. Raes (2002b), Airborne and ground based aerosol measurements in the Marseille area during ESCOMPTE (June–July 2001), paper presented at IGAC Conf., Heraklion, Crete.

Von Hoyningen-Huene, W., T. Schmidt, A. K. Chan, J. Heintzenberg, and C. Neususs (1998), Climate relevant aerosol parameters of South-East-Asian forest fire haze, *J. Aerosol Sci.*, *29*, 1259–1260.

Wang, J., et al. (2002), Clear-olumn radiative closure during ACE-Asia: Comparison of multiwavelength extinction derived from particle size and composition with results from sunphotometry, *J. Geophys. Res.*, *107*(D23), 4688, doi:10.1029/2002JD002465.

Whitby, K. T. (1978), The physical characteristics of sulfur aerosols, *Atmos. Environ.*, *12*, 135–159.

Willeke, K., and P. A. Baron (1993), Aerosol measurements: Principles, techniques and applications, Van Nostrand Reinhold, Hoboken, N. J.

S. Despiau and M. Mallet, LEPI, Université de Toulon et du Var, La Valette du Var, F-83162, France. (despiau@univ-tln.fr; mmallet@univ-tln.fr)

O. Dubovik, NASA Goddard Space Flight Center, Greenbelt, MD 20771, USA. (dubovik@aeronet.gsfc.nasa.gov)

J. P. Putaud, Joint Research Centre, Ispra, I-21020, Italy. (jean.putaud@jrc.it)

J. C. Roger, LOCL/ELICO, Université du Littoral Côte d'Opale, Dunkerque, F-62930, France. (jc@mren2.univ-littoral.fr)